Supplementary Information

Metal-free Amorphous Carbon Nitride with N-vacancies for Efficient Photocatalytic Decontamination: A Case of Peroxydisulfate-based Nonradical Oxidation Mechanism

Dandan Wei[a], Yingfei Wang[b]*, Linxi Wu[a], Dezhu Liu[a], Zheng Fang[a], Ping Chen[a], Haijin Liu[c], Wenying Lv [a], Guoguang Liu[a] *

[a] Guangdong Key Laboratory of Environmental Catalysis and Health Risk Control, Guangdong-Hong Kong-Macao Joint Laboratory for Contaminants Exposure and Health, School of Environmental Science and Engineering, Guangdong University of Technology, Guangzhou 510006, China

[b] School of Social and Ecological Civilization Teaching & Research, Party School of Guangdong Provincial Committee of C.P.C. (Chinese Academy of Governance), Guangzhou 510006, China

[c] School of Environment, Henan Normal University, Key Laboratory for Yellow River and Huaihe River Water Environment and Pollution Control, Xinxiang 453007, China

* **Corresponding Author**: liugg615@163.com (G.G. Liu); wangyf275@163.com (Y.F. Wang).

Tel: +86-20-39322547

Fax: +86-20-39322548

Supporting Information: 5 Texts, 4 Tables, and 13 Figures.

Text S1. Chemical reagents.

Ammonium acetate, urea, Sodium azide (NaN_3), L-histidine (AR), humic acid (HA, AR), Methyl alcohol (MeOH), ethanol (EtOH), isopropanol (IPA), tert-butanol (TBA) were obtained from were purchased from Aladdin Co., Shanghai, China. Ultrapure water (18.2 MΩ•cm) was used as a solvent in the adsorption experiment. Nitrogen (N_2, 99.99%), Oxygen (O_2, 99.99%) were purchased from Air Liquide. All chemicals were used as received without further purification.

Text S2. Characterization of photocatalysts.

X-ray diffractometer (XRD, Japan, Ultima VI) with Cu Kα radiation was employed to obtain the crystal structure. Scanning electron microscopy (SEM, Hitach SU8220) and transmission electron microscrpy (TEM, FEI, Thermo, Talos F200S) were utilized to investigate the morphology of the photocatalysts. The Brunauer-Emmett-Teller (BET) surface areas were measured by N_2 adsorption-desorption isotherms (Micromeritics, ASAP 2460). X-ray photoelectron spectroscopy (XPS, Thermo-Fisher, Escalab 250Xi) and element content analysis (OEA, Vario EL cube) were carried out to explore the surface and elemental composition. The stretching vibration of chemical bonds were measured on an fourier transform infrared spectrophotometer (FT-IR, Themor-Filsher, iS50R) with KBr as the reference. ESR signals were surveyed at ambient temperature by using a Bruker ESR A300 spectrometer. A UV-vis spectrometer (Shimadzu UV-3600) ($BaSO_4$ as a reference background) was used to measure the optical behavior. A transient fluorescence spectrophotometer (Edinburgh FS5; England) was used to investigate the time-resolved photoluminescence emission spectra (TRPL) and photoluminescence spectra (PL). Photocurrent measurements were carried out using an electrochemical workstation (CHI-760E, Shanghai, China). Total organic carbon (TOC) was measured by a TOC analyzer (TOC-VCPH E200V, Japan).

Text S3. Photocatalytic experiments under solar irradiation.

30 mg of ACN2 was dispersed in 50 mL of the DCF solution (6 mg/L). The suspensions were stirred in the dark for 30 min to reach adsorption-desorption equilibrium, and then 0.6 mmol PDS was added to the mixture when exposed to sunlight. The magnetic stirrer was used to ensure well-mixed conditions. Tests were conducted from 12:00 a.m. to 13:00 p.m. on sunny days in July 7 in 2023 in Guangzhou, China (N 23.04°, E 113.40°), the temperature was 28 ± 3 °C.

Text S4. Photo-electrochemistry test.

All electrochemical measurements were carried out using a CHI 760e electrochemical workstation (Chenhua Shanghai, Inc.) with a conventional three-electrode system in 0.1 M Na_2SO_4 electrolyte. An Ag/AgCl electrode, a platinum plate electrode, and an ITO electrode deposited with photocatalysts were used as the reference electrode, the counter electrode and the working electrode, respectively.

Text S5. Electron paramagnetic resonance test.

The determination of reactive species was performed using the electron paramagnetic resonance (EPR) with BRUKER model A300 measurements technique. EPR technique was utilized for the estimation of reactive species with 5,5-dimethyl-1-pyrroline-Noxide (DMPO) for the identification of sulfate radical ($SO_4^{\bullet-}$) and hydroxyl radicals (•OH), and 2,2,6,6-tetramethyl-4-piperidinol (TEMP) for $^1O_2$.

Table S1. N/C and O/C atomic rations of CN and ACN2 determined using an organic elemental analyzer (OEA) and by XPS.

Sample	OEA		XPS	
	N/C	**O/C**	**N/C**	**O/C**
CN	1.75	0.44	0.5	0.13
ACN2	1.72	0.44	0.44	0.14

Table S2. The position of N and atomic ratio for CN and ACN2 samples.

Sample	Functional group	Position (eV)	Atomic %
CN	NH_X	400	17.5
	N_{3C}	399.2	4.3
	N_{2C}	397.8	78.2
ACN2	NH_X	400.1	16.5
	N_{3C}	399.3	3.7
	N_{2C}	397.8	79.8

Table S3. Second order rate constant between organics and ROSs.

Organics	k_2(·OH)/M^{-1} s^{-1}	k_2($SO_4^{\cdot-}$)/M^{-1} s^{-1}	k_2($^1O_2$)/M^{-1} s^{-1}	k_2($O_2^{\cdot-}$)/M^{-1} s^{-1}	Ref.
BA	4.2×10^9	1.2×10^9	-	-	[1]
NB	3.9×10^9	$< 10^6$	-	-	[1]
FFA	1.5×10^{10}	-	1.2×10^8	-	[2, 3]
NBT	-	-	-	5.8×10^4	[4]

Table S4. Kinetic analysis of emission decay for the CN and ACN2.

Sample	τ_1 (ns)	Rel.%	τ_2 (ns)	Rel.%	τ_3 (ns)	Rel.%	τ_{ave} (ns)
CN	0.67	22.18	2.62	42.46	9.92	35.35	4.77
ACN2	0.17	59.88	1.47	25.44	6.32	14.68	1.40

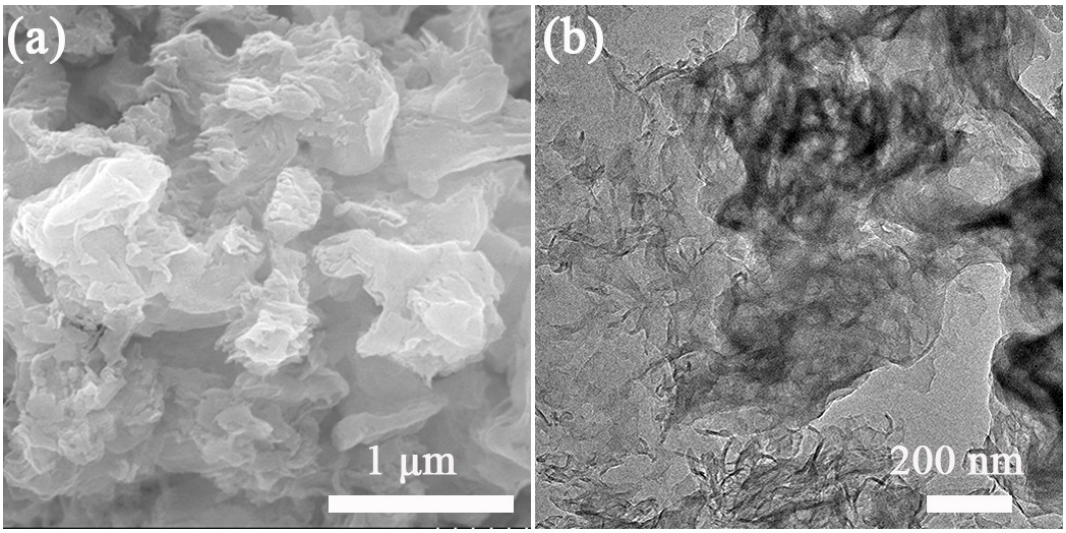

Fig. S1. (a) SEM and (b) TEM of CN.

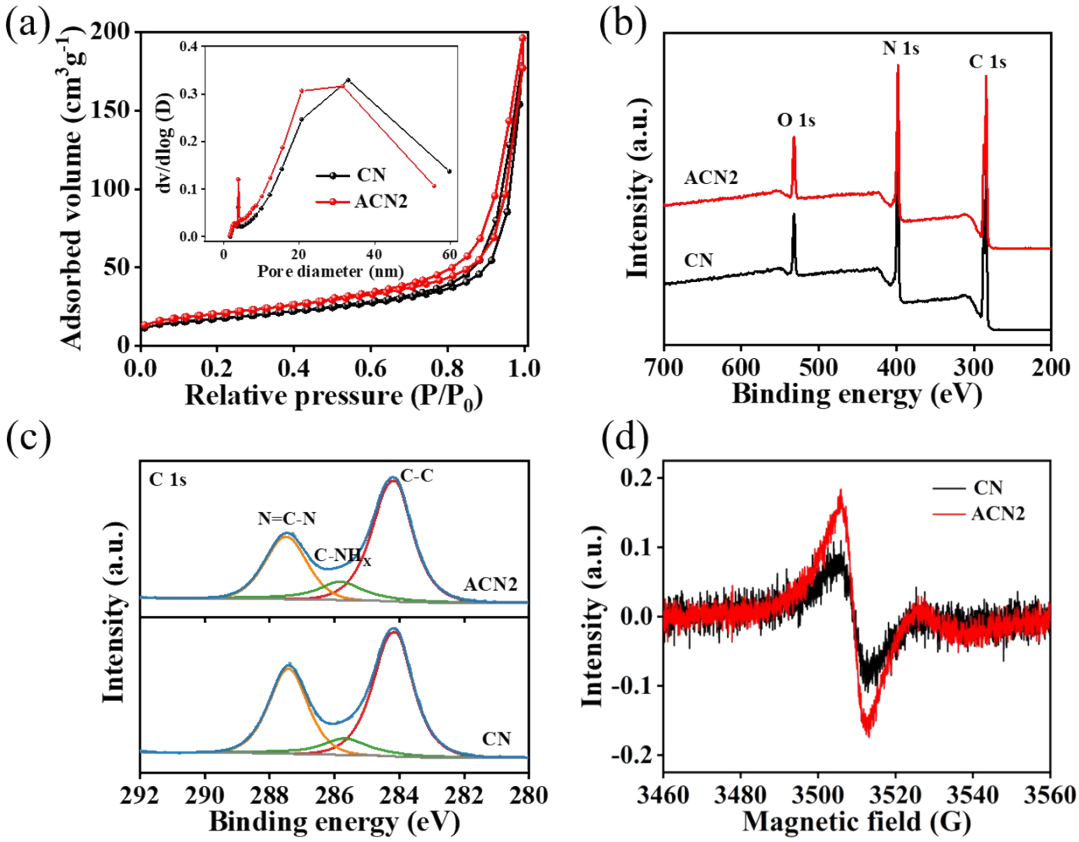

Fig. S2. (a) Nitrogen adsorption-desorption isotherms, (b) XPS survey spectra, (c) C 1s XPS spectra, and (d) EPR spectra of CN and ACN2.

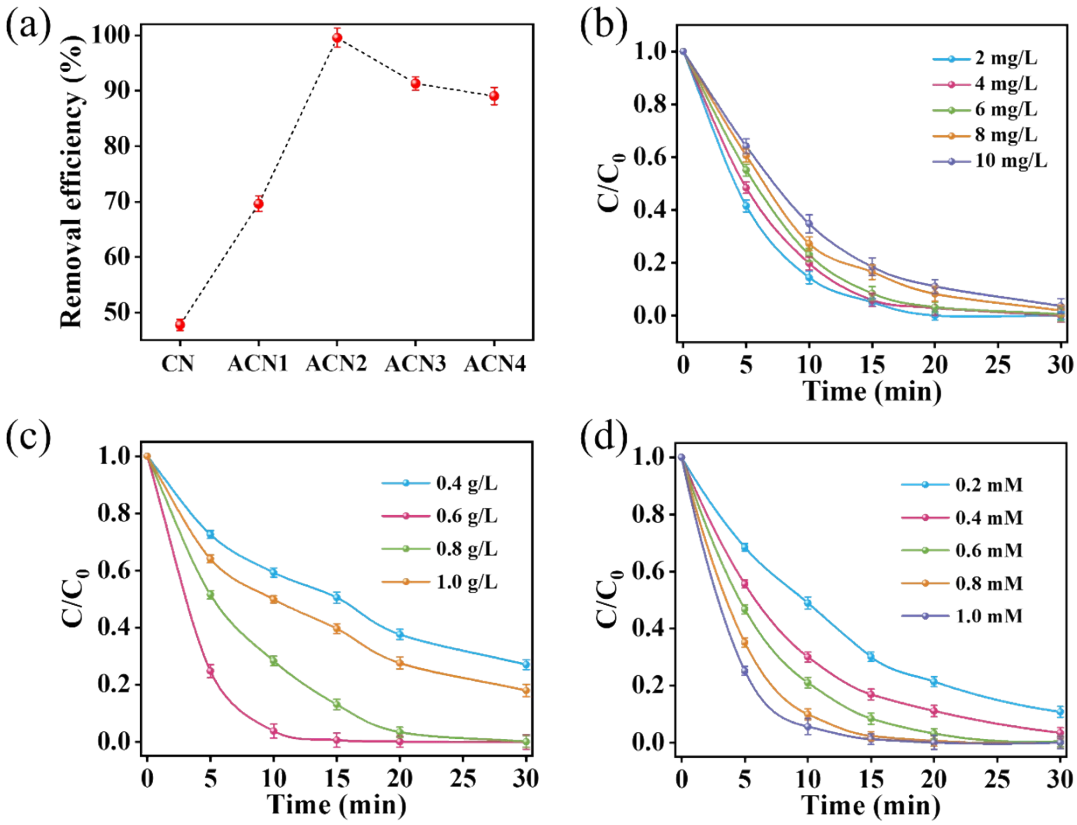

Fig. S3. (a) Effects of ammonium acetate concentration, (b) DCF concentration, (c) ACN2 concentration, and (d) PDS concentration on DCF degradation in PDS/ACN2 system.

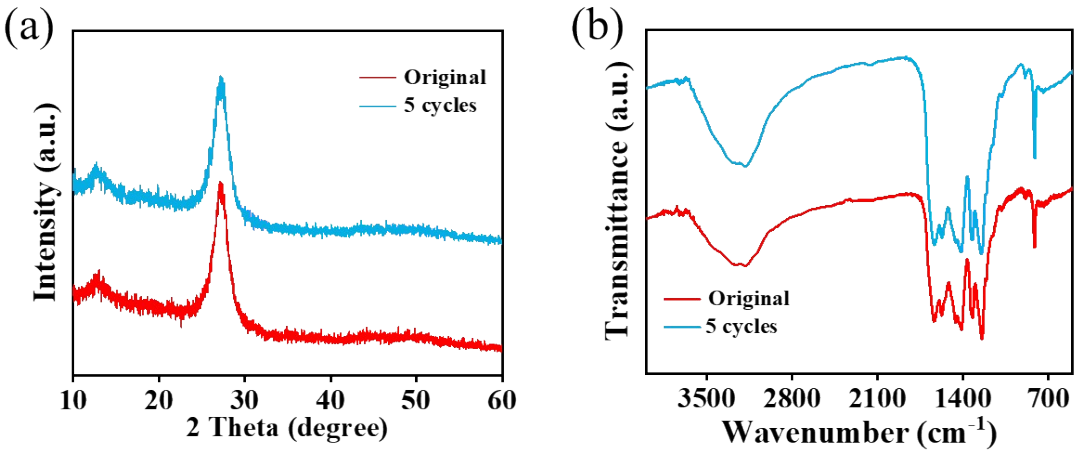

Fig. S4. (a) XRD patterns and (b) FTIR spectra for fresh and used ACN2.

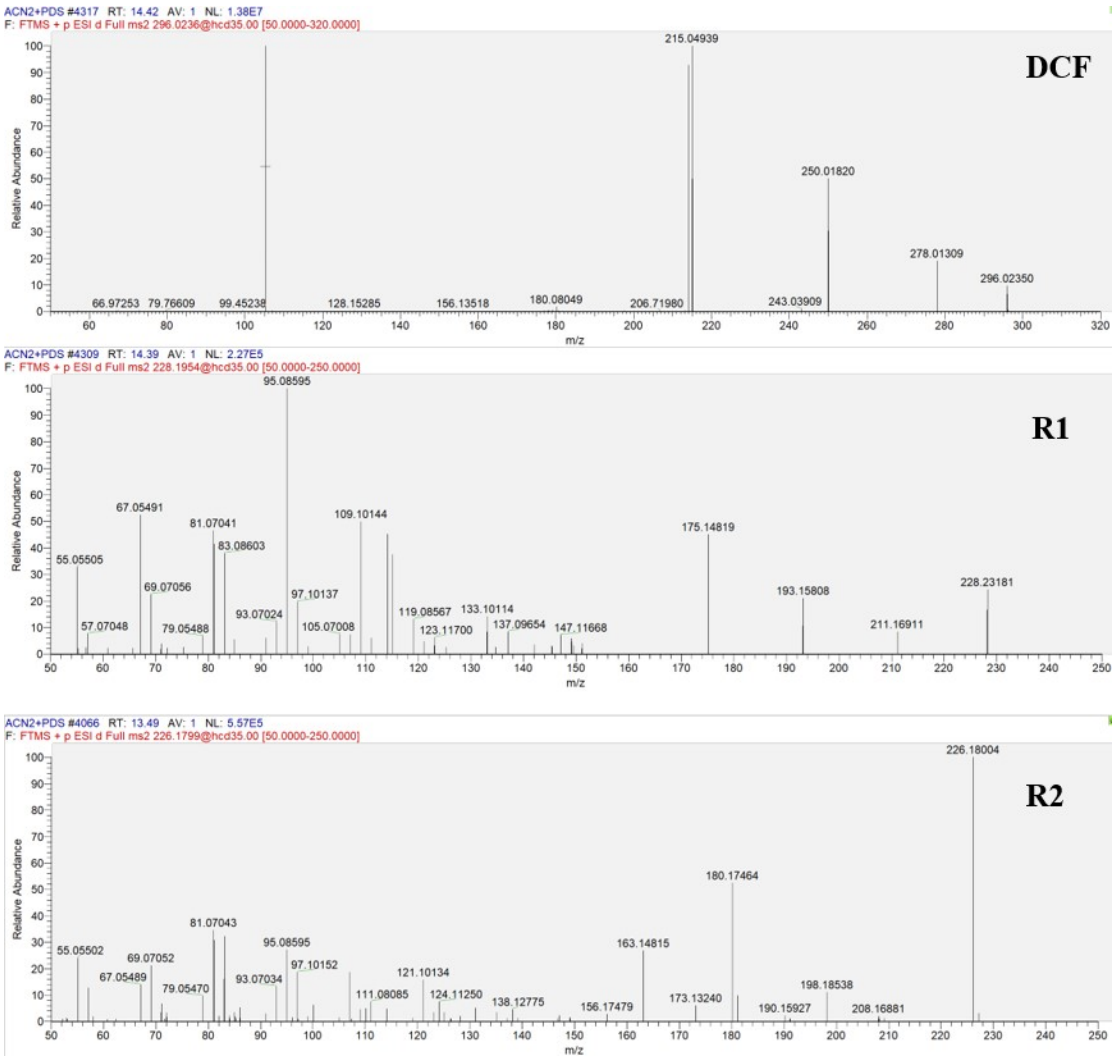
ACN2+PDS #4317 RT: 14.42 AV: 1 NL: 1.38E7
F: FTMS + p ESI d Full ms2 296.0236@hcd35.00 [50.0000-320.0000]
DCF
215.04939
250.01820
278.01309
296.02350
66.97253
79.76609
99.45238
128.15285
156.13518
180.08049
206.71980
243.03909
Relative Abundance
m/z
ACN2+PDS #4309 RT: 14.39 AV: 1 NL: 2.27E5
F: FTMS + p ESI d Full ms2 228.1954@hcd35.00 [50.0000-250.0000]
R1
95.08595
67.05491
81.07041
109.10144
175.14819
83.08603
55.05505
69.07056
97.10137
193.15808
228.23181
93.07024
119.08567
133.10114
57.07048
79.05488
105.07008
123.11700
137.09654
147.11668
211.16911
Relative Abundance
m/z
ACN2+PDS #4066 RT: 13.49 AV: 1 NL: 5.57E5
F: FTMS + p ESI d Full ms2 226.1799@hcd35.00 [50.0000-250.0000]
R2
226.18004
180.17464
81.07043
95.08595
163.14815
55.05502
69.07052
97.10152
121.10134
198.18538
67.05489
79.05470
93.07034
111.08085
124.11250
138.12775
156.17479
173.13240
190.15927
208.16881
Relative Abundance
m/z

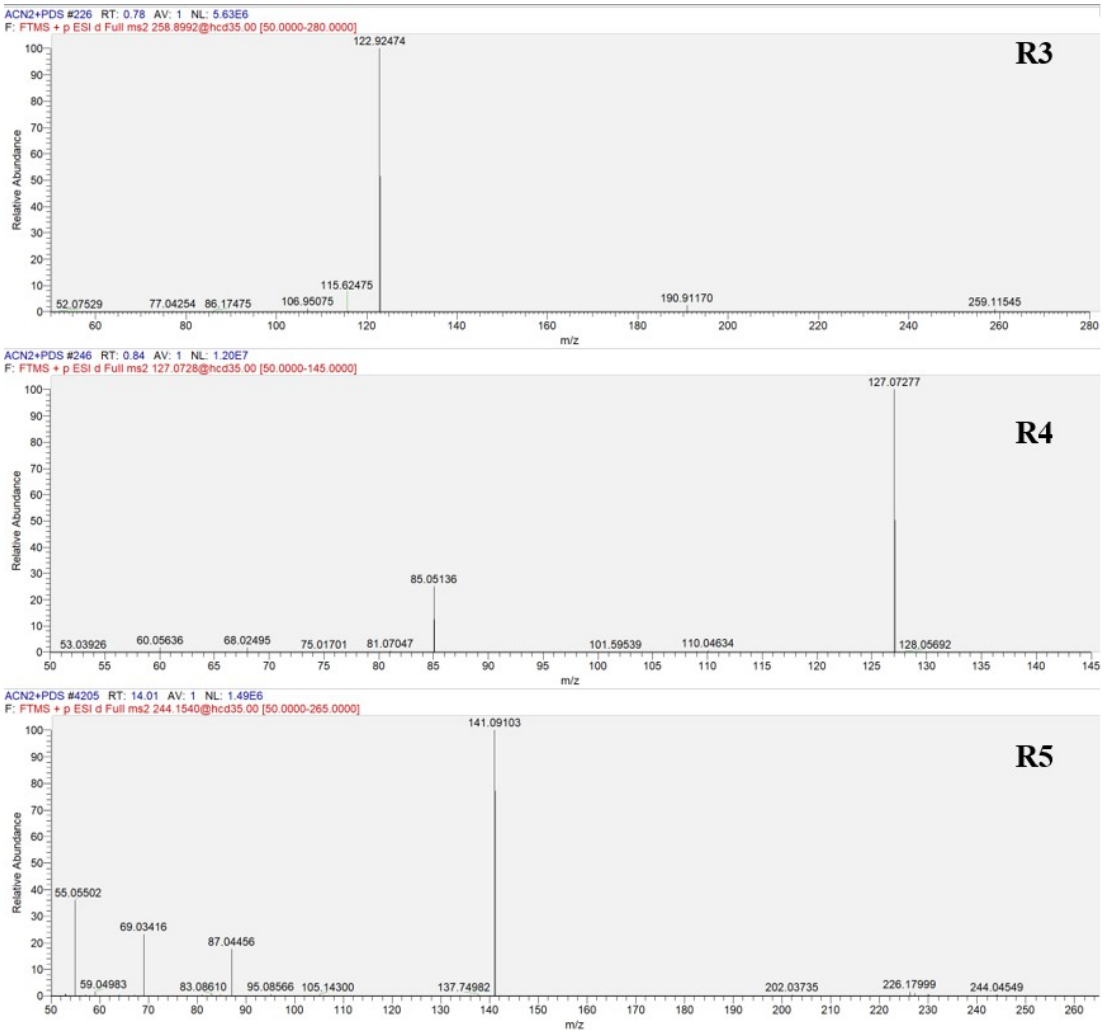
ACN2+PDS #226 RT: 0.78 AV: 1 NL: 5.63E6
F: FTMS + p ESI d Full ms2 258.8992@hcd35.00 [50.0000-280.0000]
122.92474
115.62475
52.07529
77.04254
86.17475
106.95075
190.91170
259.11545
Relative Abundance
m/z
R3
ACN2+PDS #246 RT: 0.84 AV: 1 NL: 1.20E7
F: FTMS + p ESI d Full ms2 127.0728@hcd35.00 [50.0000-145.0000]
127.07277
85.05136
53.03926
60.05636
68.02495
75.01701
81.07047
101.59539
110.04634
128.05692
Relative Abundance
m/z
R4
ACN2+PDS #4205 RT: 14.01 AV: 1 NL: 1.49E6
F: FTMS + p ESI d Full ms2 244.1540@hcd35.00 [50.0000-265.0000]
141.09103
55.05502
69.03416
87.04456
59.04983
83.08610
95.08566
105.14300
137.74982
202.03735
226.17999
244.04549
Relative Abundance
m/z
R5

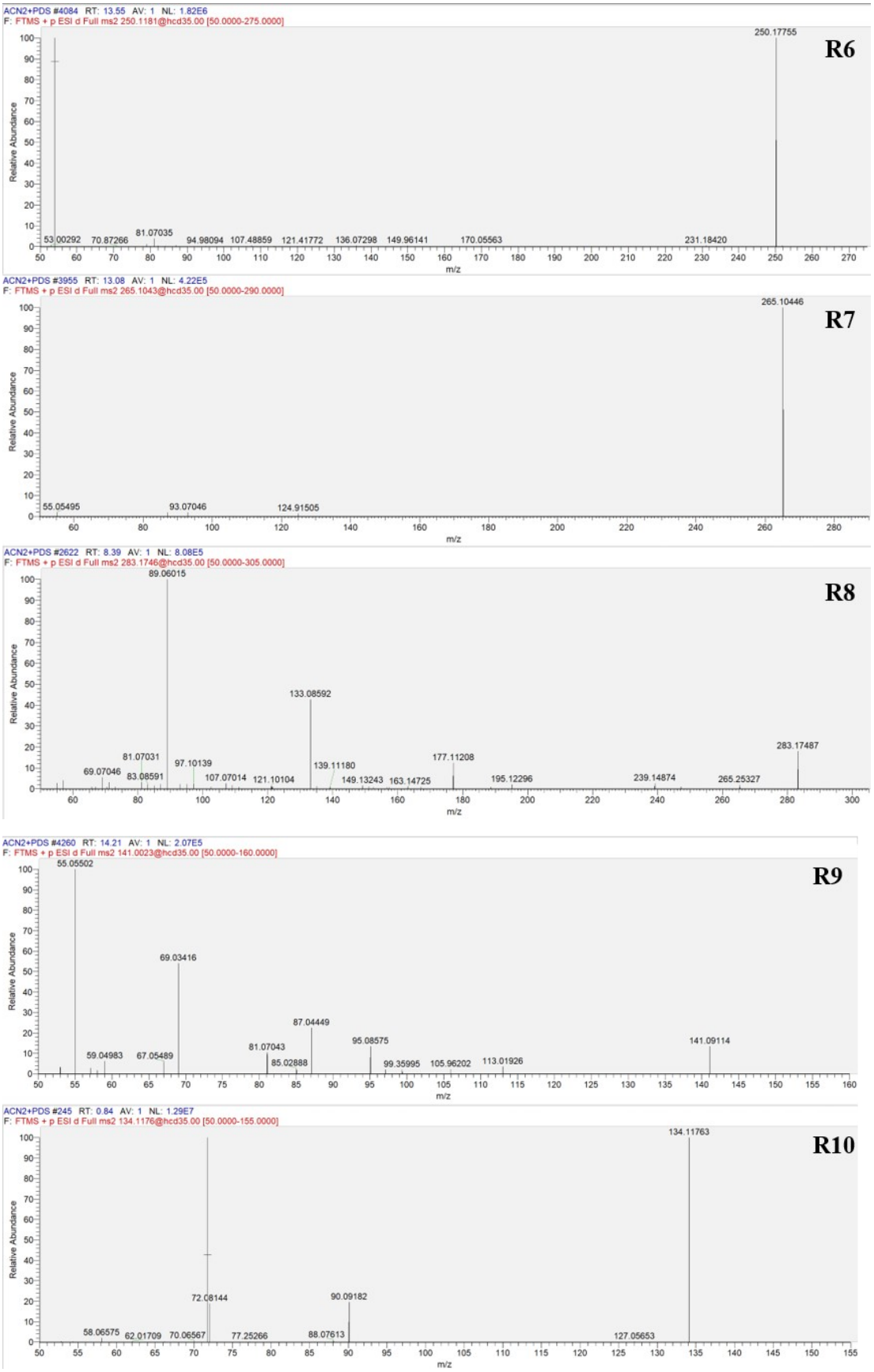

Fig. S5. DCF degradation intermediates in the ACN2/PDS system.

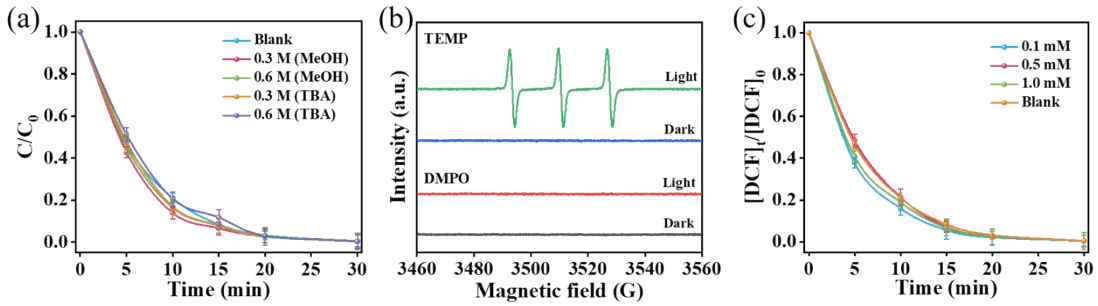

Fig. S6. (a) Quenching experiments of MeOH and TBA with different concentrations; (b) EPR spectra of •OH, $SO_4^{\bullet-}$, and $^1O_2$ in ACN2/PDS/DCF system; (c) removal of DCF under the different concentrations of FFA. Experimental conditions: $[DCF]_0$ = 6 mg/L; $[catalyst]_0$ = 0.6 g/L; $[PDS]_0$ = 0.6 mM; $[pH]_0$ = 5.6.

ESR experiments using 2,2,6,6-Tetramethyl-4-piperidinol (TEMP) as a spin trap for capturing $^1O_2$ was then performed to provide more evidences.[5] Interestingly, a strong triplet signal corresponding to TEMPO (2,2,6,6-tetramethylpiperidine-N-oxyl) was observed, which was always attribute to the formation of TEMP-$^1O_2$ adducts (**Fig. S6b**). This is contrary to the results of quenching experiment. Previous studies have demonstrated that a single electron transfer reaction can occur between TEMP and excited sensitizers to form $TEMP^{+\cdot}$, which could also generate TEMPO after deprotonation and reaction with dissolved oxygen.[6] Therefore, the TEMPO signal observed in the ACN2/PDS system may not indicate the formation of $^1O_2$.

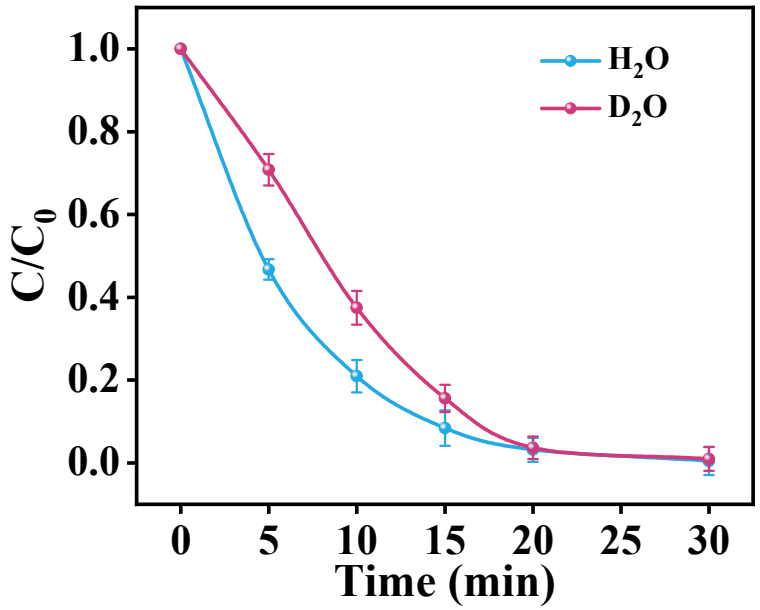

Fig. S7. Degradation performances of DCF in D_2O and H_2O.

The degradation rate of DCF in D_2O did not increase than in H_2O, which was inconsistent with the usual behavior as the lifetime of $^1O_2$ in D_2O (60 μs) is more than 15-fold longer than in H_2O (4 μs).[7] It was concluded that $^1O_2$ was not generated during the activation of PDS in the ACN2/PDS system.

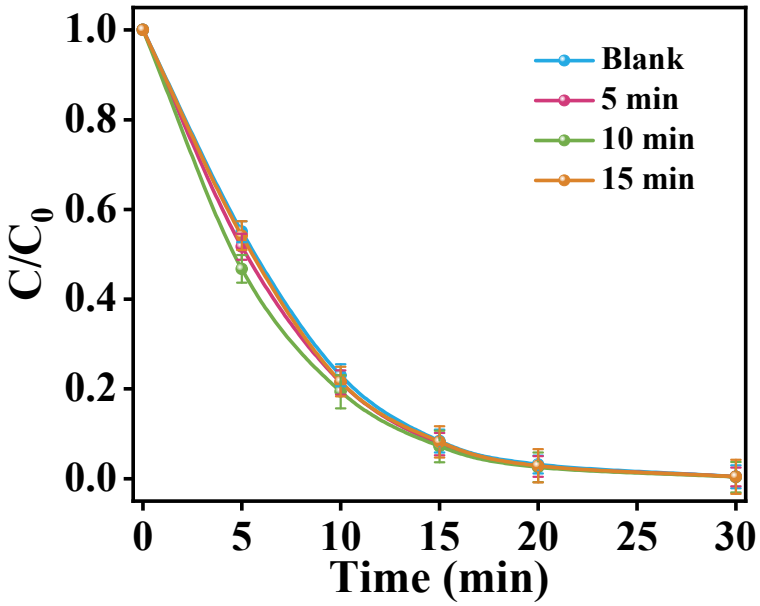

Fig. S8. Premixing ACN2 and PDS on DCF degradation.

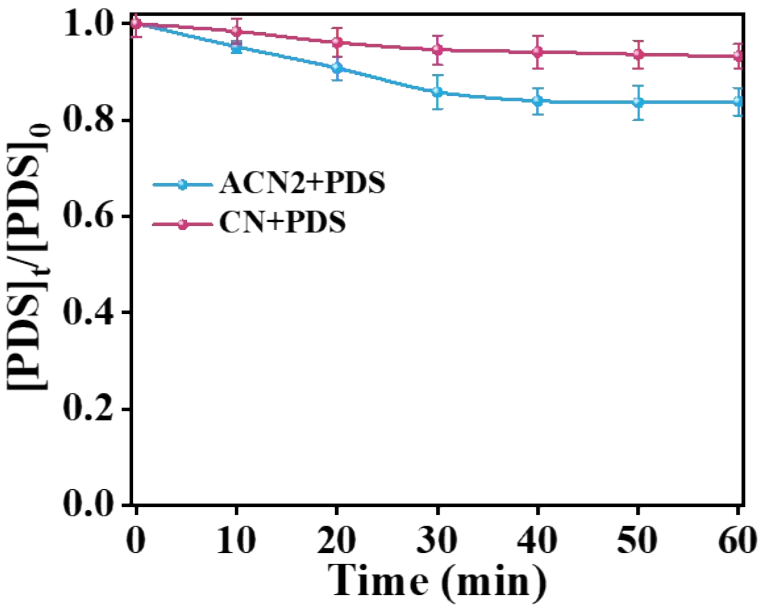

Fig. S9. PDS adsorption amounts of CN and ACN2.

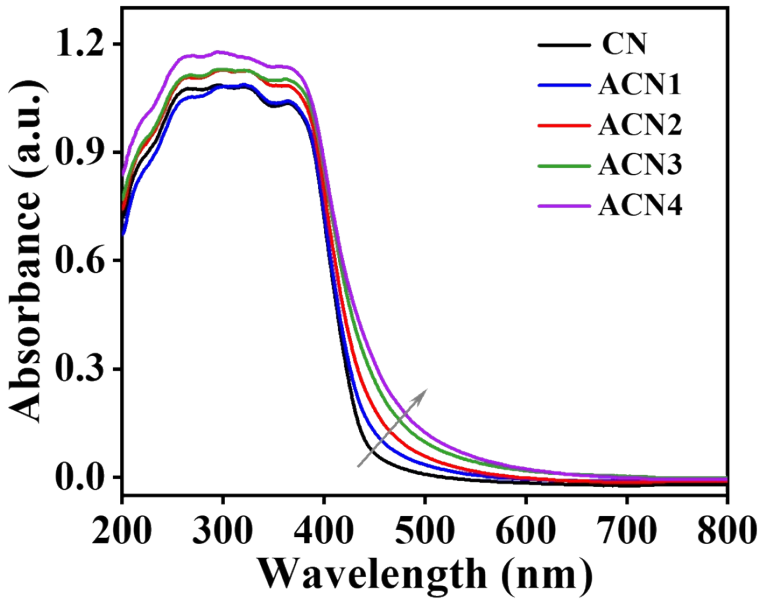

Fig. S10. UV-vis diffuse reflectance spectra of CN and ACNx samples.

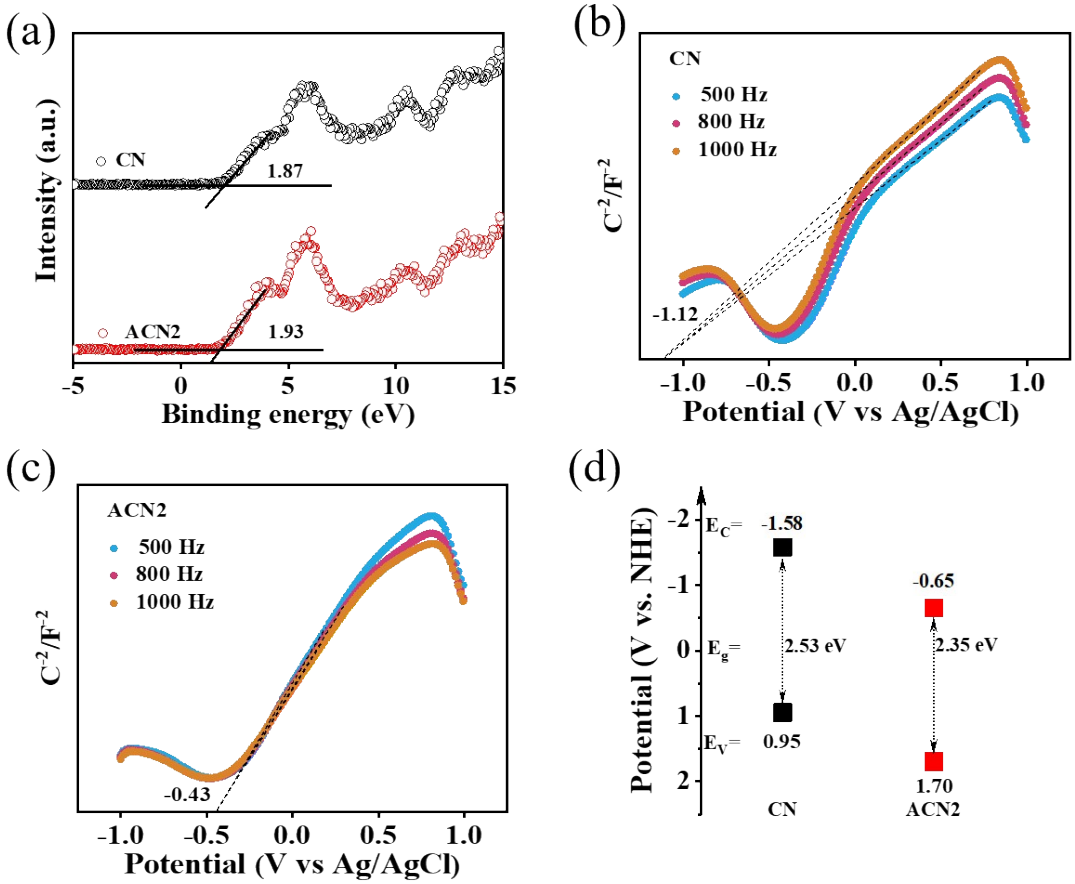

Fig. S11. (a) XPS valence band spectra, (b, c) Mott-Schottky plots, and (d) band gap structures of CN and ACN2.

The corresponding band gaps are determined from the intercept of tangents to the plot of $(\alpha h\nu)^{1/2}$ vs. photoenergy (inset in **Fig. 6a**). [8, 9] The bandgap (Eg) of ACN2 was calculated to be about 2.35 eV, which is 0.18 eV less than that of pristine CN (2.53 eV). In order to define the corresponding conduction band (CB) and valence bands (VB) position, Mott-Schottky plots and VB-XPS spectra were performed (**Fig. S11 a-c**).[10] The flat-band potentials of pristine CN and ACN2 are -1.12 and -0.43 V versus Ag/AgCl or -0.92 and -0.23 V versus NHE, respectively. Furthermore, combining with the result of VB-XPS spectra, the (VB) can be estimated to be +0.95 V versus NHE for pristine CN and +1.7 V versus NHE for ACN2. Therefore, in combination with the DRS results above, the CB position of CN and ACN2 are -1.58 and -0.65 V (Vs. NHE), respectively.

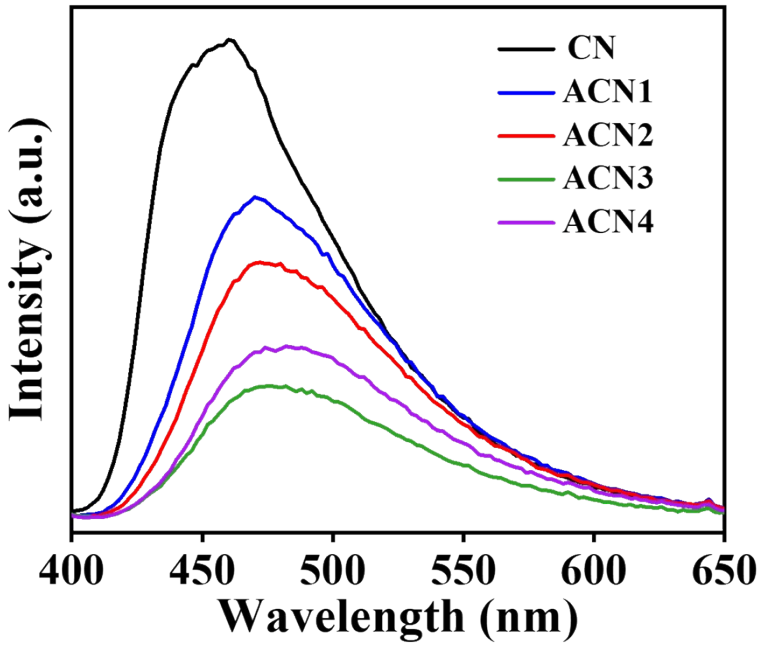

Fig. S12. Photoluminescence spectra of CN and ACNx samples.

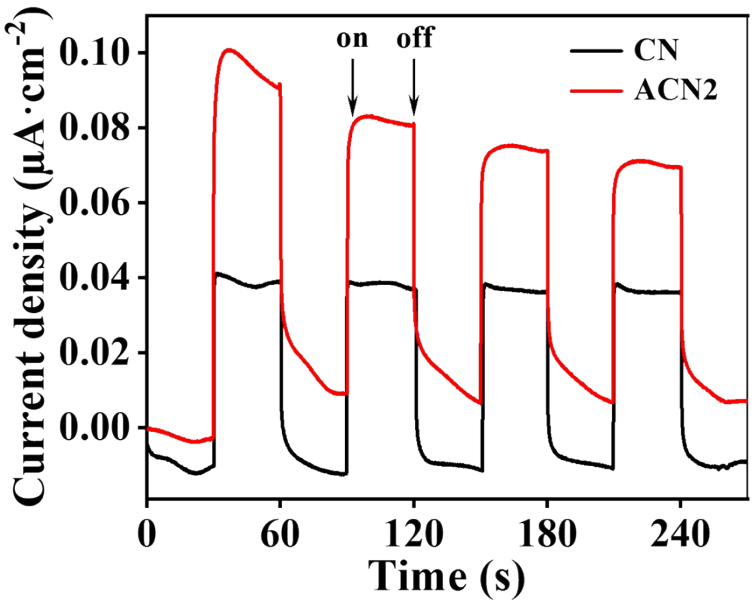

Fig. S13. Transient photocurrent spectra between CN and ACN2.

References

1. S. Zhu, X. Li, J. Kang, X. Duan and S. Wang, Persulfate activation on crystallographic manganese oxides: mechanism of singlet oxygen evolution for nonradical selective degradation of aqueous contaminants, *Environ. Sci. Technol.*, 2019, **53**, 307-315.
2. C. Minero, G. Mariella, V. Maurino, D. Vione and E. Pelizzetti, Photocatalytic transformation of organic compounds in the presence of inorganic ions. 2. Competitive reactions of phenol and alcohols an a titanium dioxide-fluoride system, *Langmuir*, 2000, **16**, 8964-8972.
3. A. D. Bokare and W. Choi, Singlet-oxygen generation in alkaline periodate solution, *Environ. Sci. Technol.*, 2015, **49**, 14392-14400.
4. J. Ma, W. Lv, P. Chen, Y. Lu, F. Wang, F. Li, K. Yao and G. Liu, Photodegradation of gemfibrozil in aqueous solution under UV irradiation: kinetics, mechanism, toxicity, and degradation pathways, *Environ. Sci. Pollut. Res.*, 2016, **23**, 14294-14306.
5. K. C. Das and C. K. Das, Curcumin (diferuloylmethane), a singlet oxygen quencher, *Biochem. Biophys. Res. Commun.*, 2002, **295**, 62-66.
6. G. Nardi, I. Manet, S. Monti, M. A. Miranda and V. Lhiaubet-Vallet, Scope and limitations of the TEMPO/EPR method for singlet oxygen detection: the misleading role of electron transfer, *Free Radical Biol. Med.*, 2014, **77**, 64-70.
7. M. Scholz, R. Dedic, T. Breitenbach and J. Hala, Singlet oxygen-sensitized delayed fluorescence of common water-soluble photosensitizers, *Photochem. Photobiol. Sci.*, 2013, **12**, 1873-1884.
8. Y. Duan, Y. Wang, L. Gan, J. Meng, Y. Feng, K. Wang, K. Zhou, C. Wang, X. Han and X. Zhou, Amorphous carbon nitride with three coordinate nitrogen ($N3_C$) vacancies for exceptional nox abatement in visible light, *Adv. Energy Mater.*, 2021, **11**, 2004001.
9. Z. Lin, Y. Wu, X. Jin, D. Liang, Y. Jin, S. Huang, Z. Wang, H. Liu, P. Chen, W. Lv and G. Liu, Facile synthesis of direct Z-scheme UiO-66-NH_2/PhC_2Cu heterojunction with ultrahigh redox potential for enhanced photocatalytic Cr(VI) reduction and NOR degradation, *J. Hazard. Mater.*, 2023, **443**, 130195.
10. J. Zhong, T. Ni, J. Huang, D. Li, C. Tan, Y. Liu, P. Chen, C. Wen, H. Liu, Z. Wang, W. Lv and G. Liu, Directional utilization disorder charge via In-plane driving force of functionalized graphite carbon nitride for the robust photocatalytic degradation of fluoroquinolone, *Chem. Eng. J.*, 2022, **442**, 135943.